Grid State Estimation in Swarm Grids

Research Project Report
Master of Science in the study program *Technische Informatik*
Faculty of Information, Media and Electrical Engineering
Cologne University of Applied Sciences (TH Köln)

Submitted by:	Markus de Koster
Address:	markus.de_koster@smail.th-koeln.de

Submitted to:	Prof.Dr. EberhardWaffenschmidt

Cologne, March 14, 2023

Technology
Arts Sciences
TH Köln

Abstract

Abstract

Traditional grid state estimation in low voltage grids is performed centralized by Distribution System Operators. In order to increase the robustness of the power systems and user autonomy, this paper proposes a Swarm Grid based approach for state estimation. Data is optionally prepared by exchanging values between current and voltage vector, described as exchange operator using Principal Pivot Transform. A combination of weighted, constrained and bounded least squares algorithm is proposed as state estimation algorithm. Additionally, worst-case assumptions are presented which help to achieve reasonable estimates of the unknown grid voltages and currents used for the decentralized grid control.

Contents

List of Tables

List of Figures

1 Swarm Grid

A swarm grid consists of multiple nodes within a distribution network that together decide on which actions to take in order to guarantee a stable and safe operation of the distribution power grid. In such a swarm, all members are equal, gather information through measurements and communicate with each other. Also, nodes can request other nodes to complete actions that benefit them and the swarm grid in general.

Centralized state estimation is prone to failure in case of an outage of the Distribution System Operator (DSO) or the network towards the DSO. In such a case, regulation of controllable loads can no longer be performed by the DSO and the power grid may enter a critical state. In a swarm grid, on the other side, all nodes can individually perform a state estimation and perform control actions even in case of network failures.

For such a swarm grid to be functional, as many nodes within the distribution system as possible must be integrated. Therefore, a shared communication and decision protocol is required. However, suggestions for such a protocol are out of scope for this paper.

2 State estimation

2.1 Fundamentals

An overview of existing distribution system state estimation (DSSE) approaches is given in [1]. All approaches have in common that the calculation is performed by the DSO who then decides on which actions to take to ensure a stable operation. In this paper, performing DSSE on distributed nodes is proposed. Because of that, the availability of data greatly differs. While in centralized DSSE measurements from Smart Meters are available to the DSO, data protection laws inhibit the ability to share user specific data especially in countries with strict data protection laws such as Germany. Furthermore, our application for grid control requires that the worst case for the grid state must be covered. This is different from applications, which analyze the system state for purposes such as fault localization or loss monitoring. [1] Multiple algorithms exist for DSSE that can be categorized into two categories, Model-based algorithms and data-driven algorithms. Model-based algorithms require prior knowledge of the distribution network, such as network topology and impedances. Here, a state vector is built with either node voltages, branch currents or power. Notably, one vector needs to be complete in order for model-based algorithms to work. Therefore, if no measurement value is available for a node or branch, replacement values have to be used instead [2]. Model-based algorithms include Weighted Least Squares (WLS), Least Absolute Value (LAV), Weighted Least Absolute Value (WLAV), Least Trimmed Squares (LTS), Least Median Squares (LMS) and Generalized Maximum-likelihood (GM). Residuals are defined as in equation 1 where x is the state vector, $h(x)$ is a nonlinear function and z is the measurement vector [1] [3].

$$r = z - h(x) \tag{1}$$

Model-based algorithms with a short description and their respective objective (minimization) functions can be found in table 1. The second category of DSSE algorithms is

Algorithm	**Description**	**Objective Function**
WLS	minimize weighted squared residuals	$r^T W r$
LAV	minimize sum of absolute values	$\sum_{i=1}^{m} \lvert r_i \rvert$
WLAV	same as LAV with weights	$\sum_{i=1}^{m} w_i \lvert r_i \rvert$
LTS	minimize the j smallest squared residuals	$\sum_{i=1}^{j} {r_i}^2$
LMS	minimize median instead of sum	$median(r^T W r)$
GM	minimize Huber cost function (η) of normalized residuals (r_{S_i})	$\sum_{i=1}^{m} {w_i}^2 \eta(r_{S_i})$

Table 1 Model-based algorithms and their objective functions (in all cases minimization); W is the weight matrix (dependent on measurement errors); adapted from [1]

data-driven algorithms which themselves can be divided into four categories [4].

- *Supervised learning* uses labeled datasets to derive unknown values
- *Unsupervised learning* groups information based on similarity in unlabeled data
- *Reinforcement learning* is a technique where good performance of a model is rewarded. Thus, positive traits are reinforced
- *Ensemble Methods* that combine multiple Machine Learning (ML) algorithms to enhance performance

The authors of [4] reviewed machine learning methods found in other publications and their applications. For short-term forecasting of energy consumption the following methods were identified.

- Kalman filter
- AutoRegressive-Moving Average (ARMA)
- Long Short Term Memory Recurrent Neural Network (LSTM-RNN)
- Support Vector Machine
- Random Forests
- Extreme Learning Machine (ELM)
- Multiple Linear Regression (MLP)

While all methods above used consumption measurements collected from smart metering devices, ELM and MLP additionally used meteorological data. Kalman-based filters track changes to the system state over time. Using past measurements, estimates of unknown variables are derived or if new measurements are available a weighted average of past and

new measurements is calculated. Some authors categorize Kalman-based filters as a third category of DSSE –forecasting-aided algorithms [1]. However, since past data is used and constantly updated with freshly available measurement data to derive unknown values others classify it as an online machine learning algorithm [4].

2.2 Replacement Values

Existing model-based algorithms require a positive measurement value redundancy at each node and for the whole low voltage network [2]. However, in reality, it is expected that the number of unknown values is significantly higher than amount of available measurements. As a solution, unknown values can be replaced by replacement values. There exist two types of replacement values, virtual measurements and pseudo measurements. Virtual measurements are those that for simulation purposes show no measurement error such as current values for nodes without energy consumption or production, often called Zero Injection Busses (ZIB) [5]. Pseudo measurements can be generated through statistical and probabilistic algorithms such as Gaussian Mixture Models or Expectation Maximization, through learning based algorithms such as deep neural networks (DNN) or Parallel Distribution Processing (PDP) based on historical data [1]. Here, for pseudo measurements node currents are set to zero. This is the worst case for the interconnecting lines and thus relevant for our application. If there is an excess of unknown values, one has to select, whether a value is put into the batch of those, that will be calculated from the measurements, or whether it will be set to a pseudo or virtual measurement value. Even if the process of selection is often clear to a skilled user, it is not always straightforward for an automated process. It will be described in chapter 3.

2.3 Different Measurement Types

In traditional supervisory control and data acquisition (SCADA) systems, data is obtained through remote telemetry units (RTUs) with measurements taken non-synchronized. Recently, phasor data concentrators (PDCs) are used to aggregate synchronized measurements from phasor measurement units (PMUs) that are also sampled at a higher rate than conventional measurements. Using both types of measurements poses the problem of time skewness where sampling rates differ and measurements are taken at different time instances. In order to accurately capture the system state, measurements need to be synchronized through GPS or time servers. [6] models the uncertainty of the delayed time as probability density function and then uses augmented state Kalman filter to solve the problem of delayed measurements. For this work, measurements were only taken synchronized in a simulation environment.

2.4 Notation and preliminaries

Nodes will be referred to as measurement busses, if – at that node – measurements are taken, as estimation busses if its values are calculated and lastly as zero injection busses if virtual measurements are applied. The grid topology is assumed to be known either through manual input or through topology estimation. Thus, also the admittance matrix

is available. Further, the grid topology contains information about whether a node is capable of feeding into the network. In a first iteration, only radial networks are considered. However, the algorithm can also be applied to meshed networks. For simulation purposes, grid topologies were generated in form of binary trees with restrictions that measurement busses may only be at the end of a line and estimation busses only at the end of a line or immediately before measurement busses. This shall represent public and private electric vehicle charging stations, and households. Finally, the phase shift at a slack node is assumed to be known (typically zero).

2.5 Algorithm

In the proposed algorithm of this paper, a combination of node voltages and branch currents can be used as the state vector. With only a limited number of known values, the voltage and current vectors each are incomplete. A model-based approach is used for DSSE. Equation 2 shows the matrix form of Ohm's Law for a single phase, symmetrical system, where $\vec{I}$ are all node currents, $\vec{U}$ are the node voltages and A is the admittance matrix.

$$\vec{U} \cdot A = \vec{I} \tag{2}$$

In our case, however, not all node voltages are known, and some node currents are already known. To solve this problem, rows can be extracted from equation 2 resulting in equation 3 where γ, β are those row indices of known values in $\vec{U}$, $\vec{I}$ and $\vec{\bar{\gamma}}$, $\vec{\bar{\beta}}$ row indices of unknown values in $\vec{U}$, $\vec{I}$ respectively.

$$A[\beta, \gamma] \cdot \vec{U}[\gamma] - \vec{I}[\beta] = -A[\beta, \bar{\gamma}] \cdot \vec{U}[\bar{\gamma}] \tag{3}$$

This results in a linear equation system with only known values on the left and part of the admittance matrix and all unknown values in $\vec{U}$ on the right. Using WLS the unknown values in $\vec{U}$ can be determined with weights assigned according to measurement accuracies.

2.5.1 Transformation using Principal Pivot Transform

A different approach for calculating unknown values in $\vec{U}$ was evaluated during work on this paper. Here, for those rows with existing current measurement values β and non-existent voltage values $\bar{\gamma}$ elements are exchanged between $\vec{U}$ and $\vec{I}$ resulting in two new vectors $\vec{X}$ and $\vec{Y}$. This process also known as *exchange operator* requires transforming the matrix using Principal Pivot Transform (PPT) as shown in equation 4.

$$\vec{Y} \cdot ppt(A, \alpha) = \vec{X} \tag{4}$$

Here, the indices of exchange are noted in α and those that have not been changed are by definition noted in $\bar{\alpha}$. Using these indices, four submatrices $A[\alpha]$, $A[\alpha, \bar{\alpha}]$, $A[\bar{\alpha}, \alpha]$ and $A[\bar{\alpha}]$ can be extracted from A, where the first parameter is row index and the second parameter column index. If only one parameter is given, row and column index values are identical. The PPT of matrix A with exchange indices α is defined in equation 6 with the Schur

complement defined in equation 5 [7].

$$A_{schur} = A[\bar{\alpha}] - A[\bar{\alpha}, \alpha] \cdot A[\alpha]^{-1} \cdot A[\alpha, \bar{\alpha}] \tag{5}$$

$$ppt(A, \alpha) = \begin{bmatrix} A[\alpha]^{-1} & -A[\alpha]^{-1} \cdot A[\alpha, \bar{\alpha}] \\ A[\bar{\alpha}, \alpha] \cdot A[\alpha]^{-1} & A_{schur} \end{bmatrix} \tag{6}$$

As can be seen, PPT requires inversion of the sub-matrix $A[\alpha]$ and thus no linear dependence in this sub-matrix. However, singularity in $A[\alpha]$ is unlikely since the sub-matrix contains the self-admittances on its diagonal.

In case of singularity, using a Moore Penrose Inverse is applicable under certain conditions described in equation 7 and 8 as described in [8] where $N(A)$ is the nullspace of A and A^* is the complex conjugate of A.

$$N(A[\alpha]) \subseteq N(A[\bar{\alpha}, \alpha]) \tag{7}$$

$$N(A^*[\alpha]) \subseteq N(A^*[\alpha, \bar{\alpha}]) \tag{8}$$

[9] finds a more generalized requirement for applicability of the exchange operator shown in equation 9 where $R(A)$ denotes the range space of A.

$$R(A[\alpha, \bar{\alpha}]) \subseteq R(A[\alpha]) \tag{9}$$

If a pseudo-inverse is used the algorithm is referred to as Generalized Principal Pivot Transform (GPPT).

Then, the matrix can be transformed similar to equation 3 resulting in an equation system with fewer unknowns and fewer equations than in the first approach. However, in both approaches all measurement values are used and after applying WLS both result in similar results for the voltage vector.

Nevertheless, due to the different resulting shape of the matrix when applying PPT, a minimization for overdetermined systems can be used instead of the WLS algorithm. This approach uses QR Decomposition of the matrix that results from equation 3 after applying PPT. In QR Decomposition square matrices or rectangular matrices (A) of shape $m \times n$ with $m \geq n$ can be decomposed such that $A = QR$. Hereby, in addition to weights, boundaries and constraints can be factored in. A comparison of both approaches requires standardized scenarios. However, due to complexity this is out of scope of this paper.

2.5.2 Constrained Least Squares

With the fully calculated voltage vector and the complete admittance matrix, the current vector can also be calculated. Therefore, a Constrained Least Squares algorithm (CLS) with addition of boundaries is used. A review on constrained state estimation algorithms can be found in [10]. Since the transformer is included in the distribution system all currents must add up to 0. Thus, this information was used as a constraint with an added

margin of 2%.

Initial values and standard deviations were set for each node according to table 2. The standard deviation for ZIB was assumed to be near zero as ZIB never inject any current. For measurement busses, the measurement inaccuracies depend on the type of measurement device, thus standard deviations should be set accordingly. Finally, for estimation nodes no information about measurement accuracy is available.

Additionally, upper and lower boundaries were defined based on the initial values and the

Node Type	**Current value**	**Voltage Value**	**Standard Deviation**
Measurement	as measured	as measured	dependent on device
ZIB	0A	-	0.0001
Estimation	-	-	-

Table 2 Initial values and standard deviation for each node type

standard deviation. For estimation nodes historical data can be used to obtain information about which bus is not capable of feeding into the system, i.e. a bus with only consumers. For those nodes an upper boundary of $I = 0$ was set. Likewise, a lower boundary for nodes that are sole producers was set to $I = 0$.

Notably, the algorithm may diverge from the given boundaries and constraints if no feasible solution is available within the given boundaries or constraints. Let $\vec{I_1}$ be the incomplete current vector consisting of complex currents and unknown values. Further, let $\vec{I_2}$ be the result of multiplication of the admittance matrix and the complete voltage vector $\vec{I_2} = A * \vec{U}$. For the algorithm to function with complex numbers, $\vec{I_1}$ and $\vec{I_2}$ are converted from $\mathbb{C}^n$ to $\mathbb{R}^{2n}$ by splitting real and imaginary part and appending them, resulting in $\vec{I}_{1_c}$ and $\vec{I}_{2_c}$ respectively. Then, we minimize the euclidean 2-norm given in 10.

$$||\vec{I}_{2_c} - \vec{I}_{1_c}||_2 \tag{10}$$

In case the results did not converge to a feasible solution, methods were applied to reduce the amount of unknown values as described in the following section.

Figure 1 shows a flowchart of all steps involved in the proposed state estimation algorithm. The used methods are shown in purple, results in blue, additional input values in orange. As described above, applying Principal Pivot Transform is optional.

3 Worst Case Scenarios

In general, those grids posed problematic to the algorithm that showed a lack of measurements especially towards the end of the power line. However, it is not possible to identify problematic networks based on network topology alone. The most deciding factor remains a lack of measurements.

In order to decrease the amount of unknown values, estimation busses were converted to ZIB with an assumed active current of zero. To ensure grid stability the nodes were

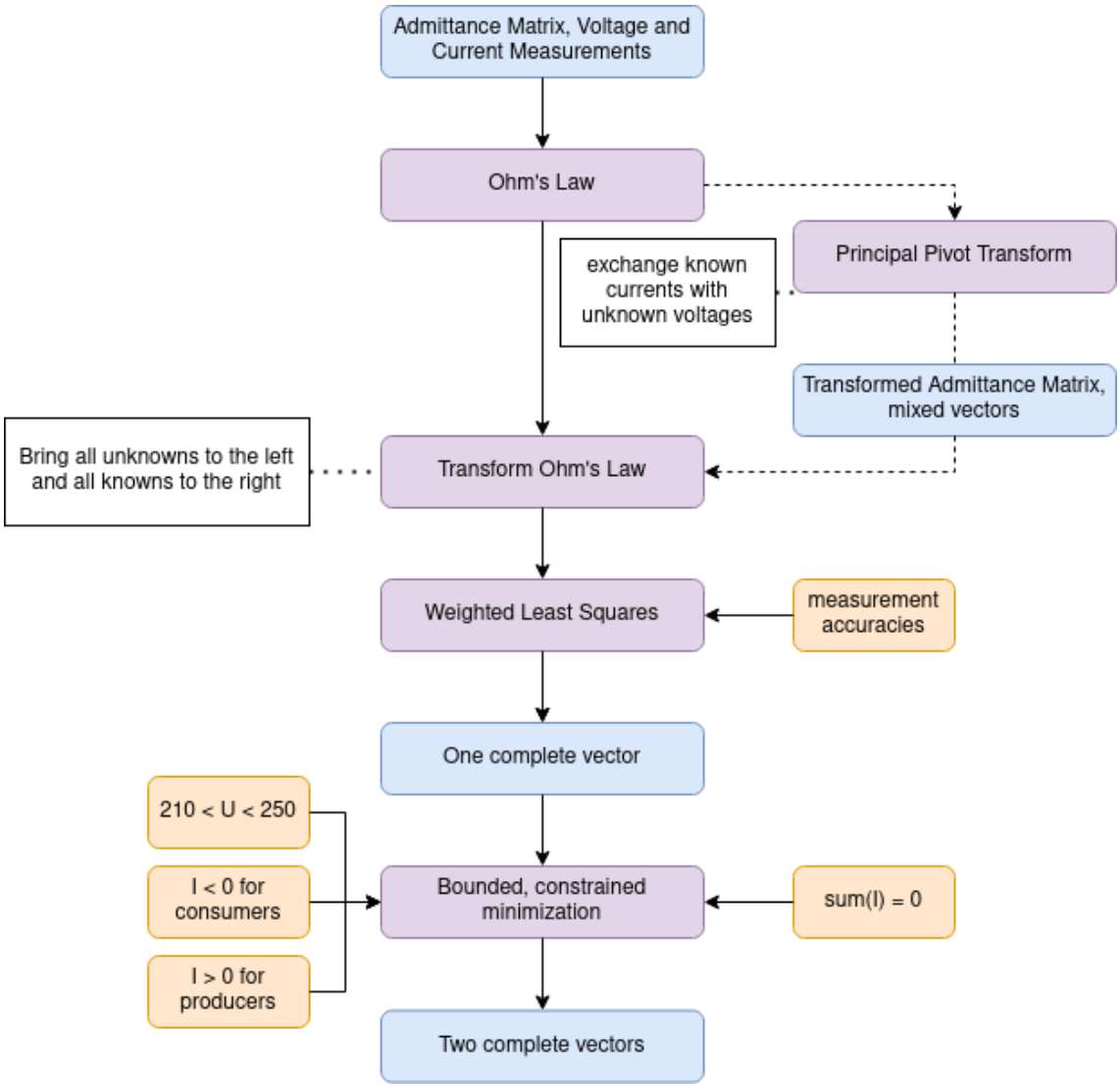

Figure 1 State Estimation flow chart as conducted in this research project

converted in such a way that a worst-case topology is generated. This was achieved by first identifying the estimation node that showed the highest divergence from the expected value. Then, starting with the identified node and moving on the line directly towards the transformer the last estimation node before the nearest measurement node was converted to a ZIB. This way, the algorithm assumes currents of the converted nodes must be assigned to the node the furthest away from the transformer. This is defined as the worst case scenario since it results in the highest possible voltage drop and line currents. Figure 2 shows an exemplary radial grid topology with only one main branch. Assuming

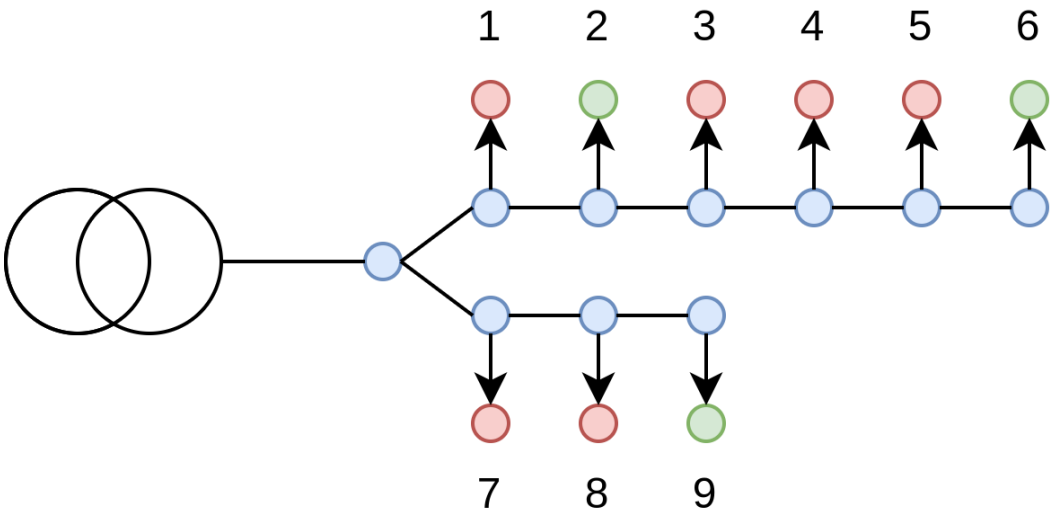

Figure 2 Exemplary Grid Topology with estimation nodes marked as red, measurement nodes as green and blind nodes as blue

the highest divergence from the expected value occurred in node 3,4 or 5, according to the proposed worst case assumption, node 3 is converted as shown in figure 3. Then, assuming

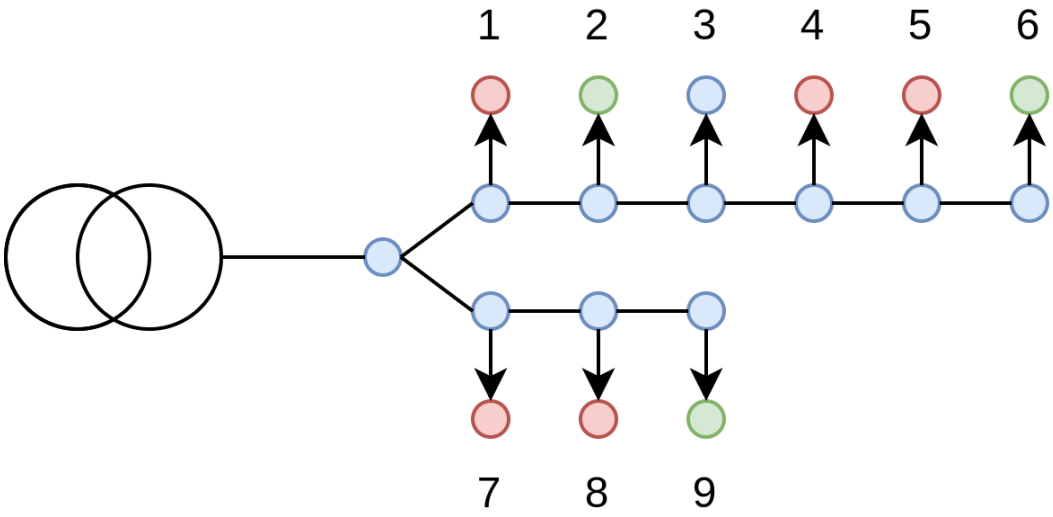

Figure 3 Exemplary Grid Topology with converted node at index 3

the highest divergence was shown at index 7 or 8, node 7 is converted as shown in figure 4.

After conversion of node 7, no further node on the lower branch can be converted. Node 8 needs to be left as estimation node so that the algorithms can assign power consumptions on that line according to worst case scenarios. The final possible conversion is shown in

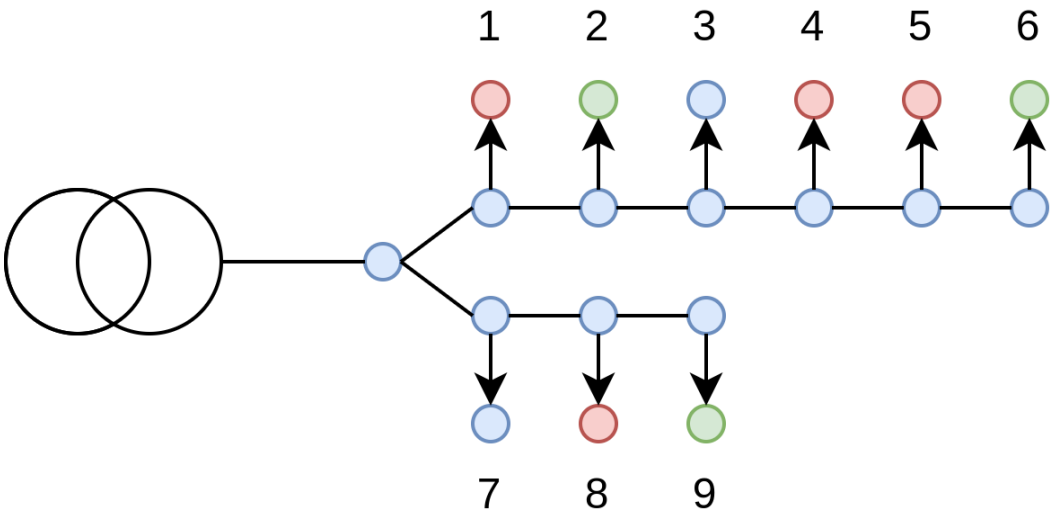

Figure 4 Exemplary Grid Topology with converted node at index 7

figure 5. According to the proposed algorithm, no further node may be converted since

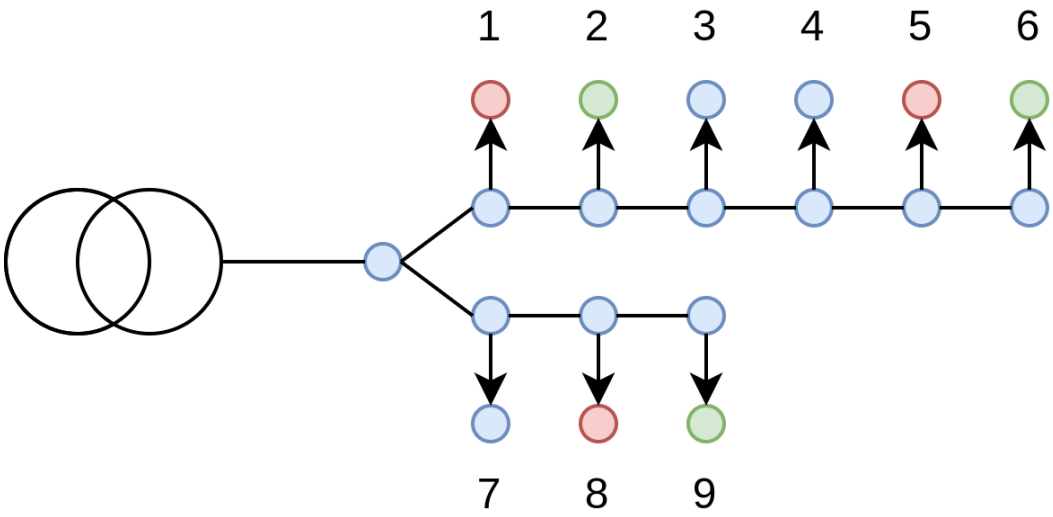

Figure 5 Exemplary Grid Topology with converted node at index 4; final configuration, no more simplifications possible

a conversion might result in unnoticed voltage drops or unnoticed transgression of the maximum line current.

4 Results

The results presented in the following section are subject to an error made in the conversion from the Per-Unit (PU) system used in *Pandapower*. However, the correct method of

conversion is shown in section 6 and the corresponding fixed results are shown in section 4.2.

4.1 Flawed Results

This section was kept in this report to explain how even major errors in the calculation may be unnoticed due to the nature of approximation algorithms. Figure 6 and 7 compare results of the state estimation to actual voltage and current values as extracted from the simulation environment. For each node the difference between the expected and actual value was calculated. Then, each of the around 21000 grids was assigned a ratio of estimation busses to measurement busses with values below 1 rounded down to the closest first decimal. Notably, due to the simulation setup not all ratios are represented equally. Finally, all grids with the same ratio value were grouped together and plotted. As can be

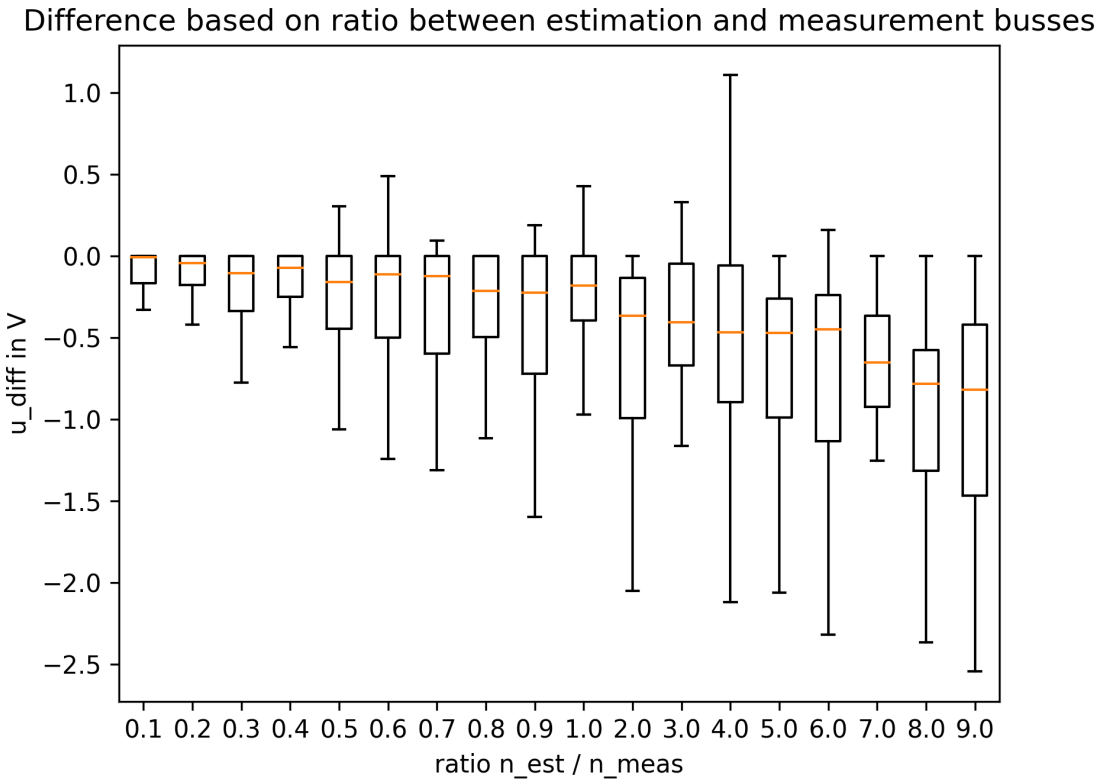

Figure 6 Flawed results: Voltage difference between expected and calculated values over ratio between amount of estimation to measurement busses

seen, for lower ratios of estimation busses to measurement busses the estimation is highly accurate. Even though the accuracy decreases with more estimation busses compared to measurement busses and thus fewer known values, the results are still fairly accurate. It shall be noted that the worst case strategies were only employed if the voltage deviated more than 20 V from 230 V. This strategy results in outliers in simulation data. Thus, outliers were removed in the final calculations. To tackle this issue, an exhaustive search for the optimal solution may be used in future work at the cost of additional computational complexity. Further, the difference from expected values does not accurately reflect worst

case scenarios as the voltage difference deviates in negative direction resulting in lower calculated voltage drops than might actually exist. Only few cases existed where the voltage difference was positive. This is also caused by the wrong conversion from the PU-System.

As can be seen, the constrained and bounded minimization forced the results into an

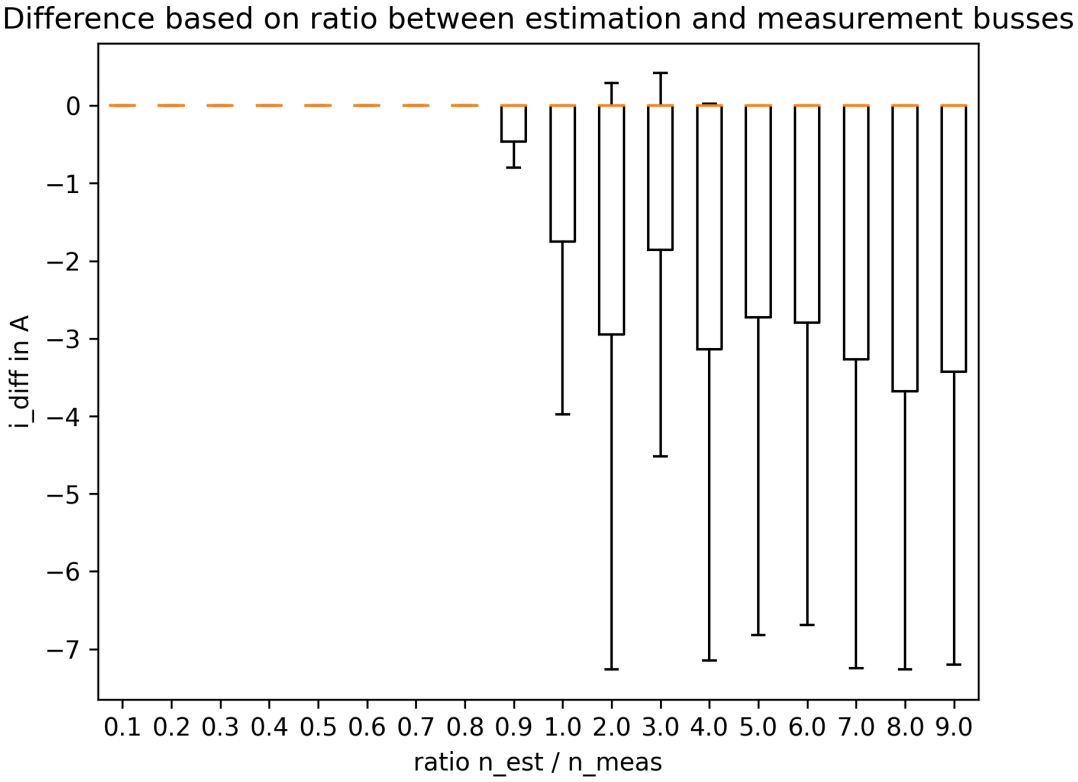

Figure 7 Flawed results: Current difference between expected and calculated values over ratio between amount of estimation to measurement busses

acceptable range and correctly depicted the expected trend that higher measurement redundancy results in better estimations. Thus, the major error in unit conversion went unnoticed for a long time.

4.2 Fixed Results

In this section, results will be shown with the fixed unit conversions. Additionally, worst case strategies were not only employed if the voltage level deviated from an acceptable range as in the flawed results above. Instead, worst case strategies were always employed until all possible node conversions were complete as described in section 3. After each conversion, the state estimation results were saved based on the updated ratio of estimation busses to measurement busses. Therefore, results in this section show not only the best estimates but all estimates relative to their respective ratios.

Thus, one can see higher overall deviations since problematic configurations were left in the data instead of only showing their best estimates after employment of worst case strategies. Additionally, the computational complexity greatly increased in this approach due to the

increased amount of state estimations computed. Because of time constraints, the following results show only 200 out of the total about 21000 grids. Figures 8, 9, 10, 11 show the

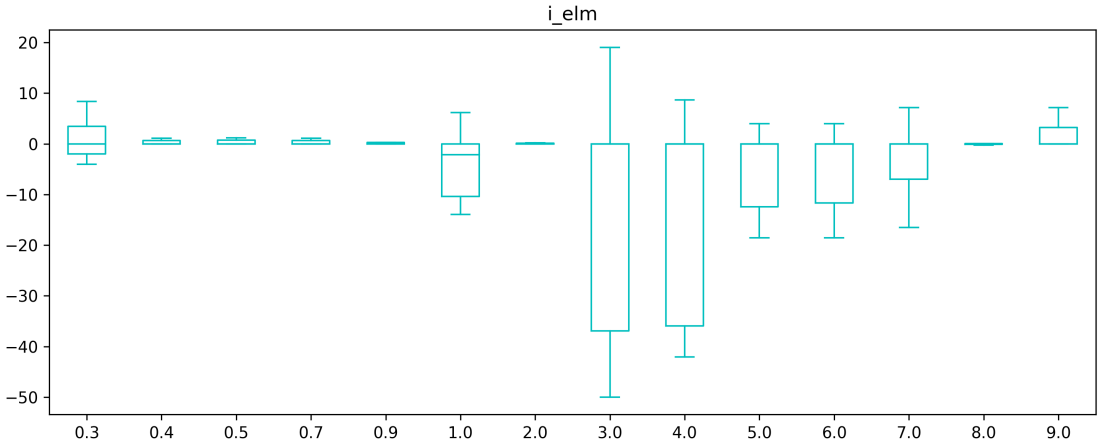

Figure 8 Fixed Results: Current difference between expected and calculated values over ratio between amount of estimation to measurement busses; with PPT applied

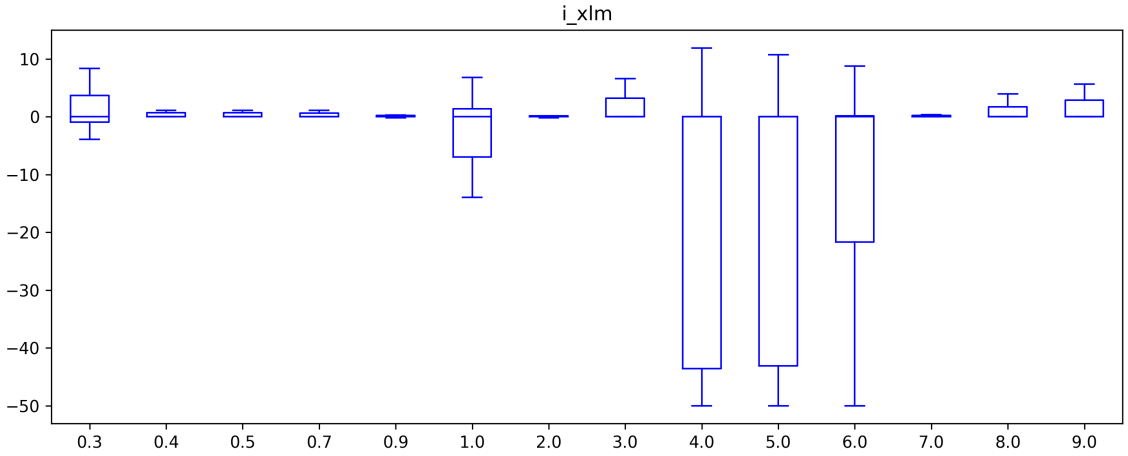

Figure 9 Fixed Results: Current difference between expected and calculated values over ratio between amount of estimation to measurement busses; without PPT applied

fixed results as a difference between expected and calculated values. In figures 8 and 10 PPT was applied first as explained in section 2.5.1. Notably, once again not all ratios are represented equally. Since always all possible conversions of estimation nodes to ZIB were included in the data, lower ratios are heavily over-represented.

In first tests, applying a constrained and bounded minimization twice, once for calculating one side of unknowns as described in chapter 2.5 and again for calculating the leftover unknowns as described in chapter 2.5.2 resulted in better overall values for ratios up to 3.

4.3 Possible improvements

Using a symmetric simplified equivalent network for low voltage systems that are mostly operated asymmetrically may result in increased errors [5]. Because of that, the calculation can be performed using symmetric components. In addition, the proposed algorithms need

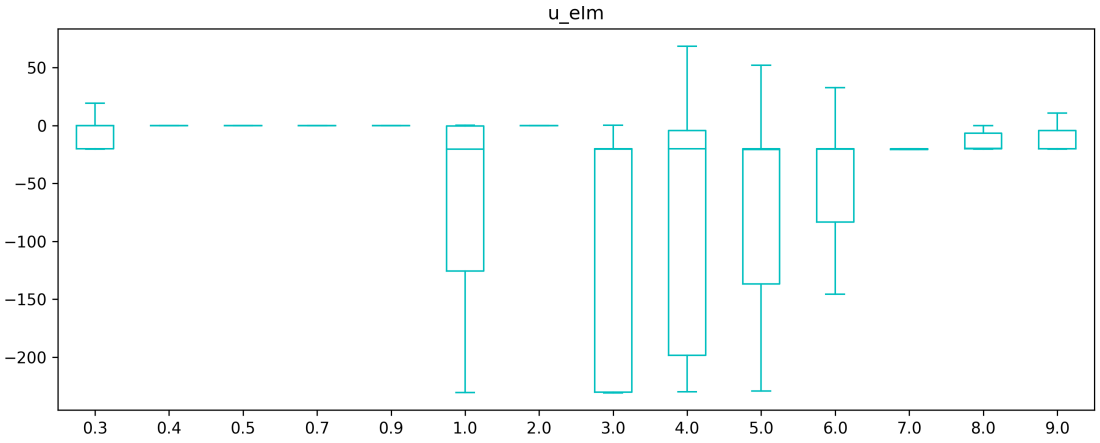

Figure 10 Fixed Results: Voltage difference between expected and calculated values over ratio between amount of estimation to measurement busses; with PPT applied

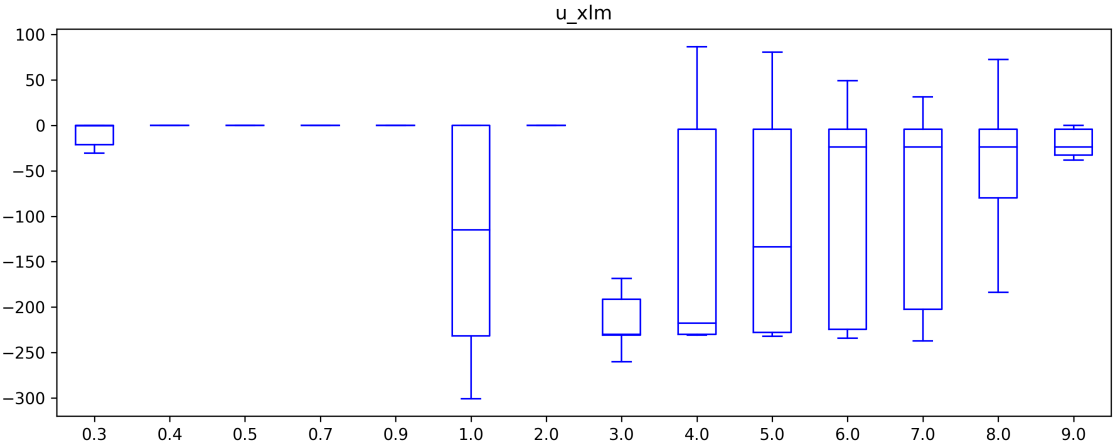

Figure 11 Fixed Results: Voltage difference between expected and calculated values over ratio between amount of estimation to measurement busses; without PPT applied

to be compared to traditional algorithms with regard to performance and accuracy. Further, estimation and measurement nodes were assigned fixed values that did not alternate throughout the simulation. Instead, load profiles should be used in future work. Finally, the proposed algorithm should be tested outside of simulations and in varying scenarios.

5 Examples

In the following section, example calculations for the above explained algorithms are given. Indices will be given starting at zero and results are trimmed to three decimal places.

$$\begin{pmatrix} u_0 \\ u_1 \\ 241.970 \\ 238.534 \\ u_4 \\ 241.694 \\ u_6 \end{pmatrix} \cdot \begin{bmatrix} 8.335 & -8.333 & 0 & 0 & 0 & 0 & 0 \\ -8.333 & 16.527 & -4.347 & 0 & 0 & -3.846 & 0 \\ 0 & -4.347 & 7.289 & -2.941 & 0 & 0 & 0 \\ 0 & 0 & -2.941 & 5.163 & -2.222 & 0 & 0 \\ 0 & 0 & 0 & -2.222 & 2.222 & 0 & 0 \\ 0 & -3.846 & 0 & 0 & 0 & 5.338 & -1.492 \\ 0 & 0 & 0 & 0 & 0 & -1.492 & 1.492 \end{bmatrix} = \begin{pmatrix} i_0 \\ 0 \\ 0 \\ 0 \\ i_4 \\ 0 \\ i_6 \end{pmatrix}$$

The equation above shows an exemplary starting point applying Ohm's Law (see equation 2) with a known admittance matrix, some known node voltages and some known currents.

5.1 Principal Pivot Transform

The node with index 1 has a known current of $i_1 = 0A$ and an unknown voltage u_1. Thus, PPT can be applied with the given index $\alpha = [1]$ Since only one index will be swapped, the principal submatrix will consist of only a single element.

$$A[\alpha] = \begin{bmatrix} a_{11} \end{bmatrix} = \begin{bmatrix} 16.527 \end{bmatrix}$$

The other submatrices can be formed accordingly with $\bar{\alpha} = [0, 2, 3, 4, 5, 6]$.

$$A[\bar{\alpha}] = \begin{bmatrix} a_{00} & a_{02} & a_{03} & a_{04} & a_{05} & a_{06} \\ a_{20} & a_{22} & a_{23} & a_{24} & a_{25} & a_{26} \\ a_{30} & a_{32} & a_{33} & a_{34} & a_{35} & a_{36} \\ a_{40} & a_{42} & a_{43} & a_{44} & a_{45} & a_{46} \\ a_{50} & a_{52} & a_{53} & a_{54} & a_{55} & a_{56} \\ a_{60} & a_{62} & a_{63} & a_{64} & a_{65} & a_{66} \end{bmatrix} = \begin{bmatrix} 8.335 & 0 & 0 & 0 & 0 & 0 \\ 0 & 7.289 & -2.941 & 0 & 0 & 0 \\ 0 & -2.941 & 5.163 & -2.222 & 0 & 0 \\ 0 & 0 & -2.222 & 2.222 & 0 & 0 \\ 0 & 0 & 0 & 0 & 5.338 & -1.492 \\ 0 & 0 & 0 & 0 & -1.492 & 1.492 \end{bmatrix}$$

$$A[\alpha, \bar{\alpha}] = \begin{bmatrix} a_{10} & a_{12} & a_{13} & a_{14} & a_{15} & a_{16} \end{bmatrix} = \begin{bmatrix} -8.333 & -4.347 & 0 & 0 & -3.846 & 0 \end{bmatrix}$$

$$A[\bar{\alpha}, \alpha] = \begin{bmatrix} a_{01} \\ a_{21} \\ a_{31} \\ a_{41} \\ a_{51} \\ a_{61} \end{bmatrix} = \begin{bmatrix} -8.333 \\ 16.527 \\ -4.347 \\ 0 \\ 0 \\ -3.846 \\ 0 \end{bmatrix}$$

Applying equation 6 results in the following matrix.

$$ppt(A, \alpha) = B = \begin{bmatrix} 4.134 & -0.504 & -2.192 & 0 & 0 & -1.939 & 0 \\ 0.504 & 0.060 & 0.263 & -0 & -0 & 0.232 & -0 \\ -2.192 & -0.263 & 6.145 & -2.941 & 0 & -1.011 & 0 \\ 0 & 0 & -2.941 & 5.163 & -2.222 & 0 & 0 \\ 0 & 0 & 0 & -2.222 & 2.222 & 0 & 0 \\ -1.939 & -0.232 & -1.011 & 0 & 0 & 4.443 & -1.492 \\ 0 & 0 & 0 & 0 & 0 & -1.492 & 1.492 \end{bmatrix}$$

Now, the exchange operator can be applied to the voltage and current vector resulting in.

$$\vec{X} = \begin{pmatrix} i_0 \\ u_1 \\ i_2 \\ i_3 \\ i_4 \\ i_5 \\ i_6 \end{pmatrix} = \begin{pmatrix} ? \\ ? \\ 0 \\ 0 \\ ? \\ 0 \\ ? \end{pmatrix}, \vec{Y} = \begin{pmatrix} u_0 \\ i_1 \\ u_2 \\ u_3 \\ u_4 \\ u_5 \\ u_6 \end{pmatrix} = \begin{pmatrix} ? \\ 0 \\ 241.970 \\ 238.534 \\ ? \\ 241.694 \\ ? \end{pmatrix}$$

5.2 Equation transformation

Bringing all unknowns to the right side and all knowns to the left side results in the following equations. With $\beta = [2, 3, 5]$, $\gamma = [1, 2, 3, 5]$, $\bar{\gamma} = [0, 4, 6]$

$$B[\beta, \gamma] \cdot \vec{Y}[\gamma] - \vec{X}[\beta] = \begin{bmatrix} -0.263 & 6.145 & -2.941 & -1.011 \\ 0 & -2.941 & 5.163 & 0 \\ -0.232 & -1.011 & 0 & 4.443 \end{bmatrix} \cdot \begin{pmatrix} 0 \\ 241.970 \\ 238.534 \\ 241.694 \end{pmatrix} - \begin{pmatrix} 0 \\ 0 \\ 0 \end{pmatrix} = \begin{pmatrix} 540.940 \\ 520.029 \\ 829.230 \end{pmatrix}$$

$$-B[\beta, \bar{\gamma}] \cdot \vec{Y}[\bar{\gamma}] = \begin{bmatrix} 2.192 & -0 & -0 \\ -0 & 2.222 & -0 \\ 1.939 & -0 & 1.492 \end{bmatrix} \cdot \begin{pmatrix} y_0 \\ y_4 \\ y_6 \end{pmatrix}$$

Therefore according to equation 3:

$$\begin{pmatrix} 540.940 \\ 520.029 \\ 829.230 \end{pmatrix} = \begin{bmatrix} 2.192 & -0 & -0 \\ -0 & 2.222 & -0 \\ 1.939 & -0 & 1.492 \end{bmatrix} \cdot \begin{pmatrix} y_0 \\ y_4 \\ y_6 \end{pmatrix}$$

If PPT is not applied, the starting equation can be immediately transformed with $\beta = [1, 2, 3, 5]$, $\gamma = [2, 3, 5]$, $\bar{\gamma} = [0, 1, 4, 6]$

$$A[\beta, \gamma] \cdot \vec{U}[\gamma] - \vec{I}[\beta] = \begin{bmatrix} -4.347 & 0.000 & -3.846 \\ 7.289 & -2.941 & 0.000 \\ -2.941 & 5.163 & 0.000 \\ 0.000 & 0.000 & 5.338 \end{bmatrix} \cdot \begin{pmatrix} 241.970 \\ 238.534 \\ 241.694 \end{pmatrix} - \begin{pmatrix} 0 \\ 0 \\ 0 \\ 0 \end{pmatrix} = \begin{pmatrix} -1981.642 \\ 1062.234 \\ 520.029 \\ 1290.374 \end{pmatrix}$$

$$-A[\beta, \bar{\gamma}] \cdot \vec{U}[\bar{\gamma}] = \begin{bmatrix} 8.333 & -16.527 & -0.000 & -0.000 \\ -0.000 & 4.347 & -0.000 & -0.000 \\ -0.000 & -0.000 & 2.222 & -0.000 \\ -0.000 & 3.846 & -0.000 & 1.492 \end{bmatrix} \cdot \begin{pmatrix} u_0 \\ u_1 \\ u_4 \\ u_6 \end{pmatrix}$$

Once again, according to equation 3

$$\begin{pmatrix} -1981.642 \\ 1062.234 \\ 520.029 \\ 1290.374 \end{pmatrix} = \begin{bmatrix} 8.333 & -16.527 & -0.000 & -0.000 \\ -0.000 & 4.347 & -0.000 & -0.000 \\ -0.000 & -0.000 & 2.222 & -0.000 \\ -0.000 & 3.846 & -0.000 & 1.492 \end{bmatrix} \cdot \begin{pmatrix} u_0 \\ u_1 \\ u_4 \\ u_6 \end{pmatrix}$$

Notably, in both cases (with PPT and without PPT), the system is well-determined. With PPT there are 3 equations and 3 unknowns without any linear dependence. Without PPT there are 4 equations and 4 unknowns without any linear dependence. As explained in section 2.5.1 in case of underdetermined systems, it is only possible to apply a QR-Decomposition after applying PPT first due to the shape of the resulting matrix. Also, solving a system with fewer equations and fewer unknowns might be beneficial in some cases (linear dependence). Thus, there might be some benefit to applying PPT first.

Now, a weighted least squares can be used to approximately solve the above equation. However, due to unknown measurement accuracies, in this specific case all weights were equal. Using *numpy* least squares algorithm results in $y_0 = 246.759$, $y_4 = 234.013$, $y_6 = 234.973$ with PPT and in $u_0 = 246.759$, $u_1 = 244.313$, $u_4 = 234.013$, $u_6 = 234.973$ without using PPT first. For the sake of simplicity, in the following the values calculated from using PPT first will be used. However, the algorithm is applicable to both cases.

The results of the weighted least squares can be filled in $\vec{Y}$ which is now complete.

$$\vec{Y} = \begin{pmatrix} 246.759 \\ 0 \\ 241.970 \\ 238.534 \\ 234.013 \\ 241.694 \\ 234.973 \end{pmatrix}$$

5.3 Constrained Least Squares

In this specific example, no conversion from complex to real numbers is necessary. Bounds for measured values were set to those values with an added deviation equal to the standard deviation of that measurement. Lower bounds are shown on the left and upper bounds on the right.

$$bounds = \begin{pmatrix} 0,50 \\ 210,250 \\ -0.001,0.001 \\ -0.001,0.001 \\ -50,0 \\ -0.001,0.001 \\ -50,0 \end{pmatrix}$$

The constrained and bounded minimization of $B * \vec{Y} = \vec{X}$ results in

$$\vec{X} = \begin{pmatrix} 20.999 \\ 244.313 \\ 0 \\ 0 \\ -10.001 \\ 0 \\ -10 \end{pmatrix}$$

Finally, the exchange operator is reversed.

$$\vec{I} = \begin{pmatrix} 20.999 \\ 0 \\ 0 \\ 0 \\ -10.001 \\ 0 \\ -10 \end{pmatrix}, \vec{U} = \begin{pmatrix} 246.759 \\ 244.313 \\ 241.970 \\ 238.534 \\ 234.013 \\ 241.694 \\ 234.973 \end{pmatrix}$$

6 Per Unit System Conversion

Voltages and admittance matrices are given in the per-unit (PU) system in *Pandapower*. This simplifies calculations especially in systems with transformers between different voltage levels. In the PU-System values are expressed relative to a defined base unit [11].

In *Pandapower* grid voltage levels *vn* and the reference apparent power for per unit system *sn* are required to transform values from and to the PU-System.

To transform an admittance matrix from the per-unit system, a reference admittance matrix is established as follows. For each combination of from (i) and to (j) bus, a reference

impedance (z_r) is calculated as shown in equation 11.

$$z_{r_{i,j}} = \frac{vn_i \times vn_j}{sn} \tag{11}$$

These reference impedances can be converted to reference admittances $y_r = 1/z_r$ and combined into a reference admittance matrix as shown in equation 12.

$$\begin{bmatrix} y_{r_{1,1}} & y_{r_{1,2}} & \cdots & y_{r_{1,n-1}} & y_{r_{1,n}} \\ y_{r_{2,1}} & y_{r_{2,2}} & \cdots & y_{r_{2,n-1}} & y_{r_{2,n}} \\ \cdots & \cdots & \cdots & \cdots & \cdots \\ y_{r_{m-1,1}} & y_{r_{m-1,2}} & \cdots & y_{r_{m-1,n-1}} & y_{r_{m-1,n}} \\ y_{r_{m,1}} & y_{r_{m,2}} & \cdots & y_{r_{m,n-1}} & y_{r_{m,n}} \end{bmatrix} \tag{12}$$

Finally, multiplying the reference admittance matrix with the per-unit admittance matrix given by *Pandapower* results in the admittance matrix.

$$Y = Y_{pu} * Y_r \tag{13}$$

References

[1] M. Fotopoulou, S. Petridis, I. Karachalios, and D. Rakopoulos, "A Review on Distribution System State Estimation Algorithms," en, *Applied Sciences*, vol. 12, no. 21, p. 11 073, Nov. 2022, ISSN: 2076-3417. DOI: 10.3390/app122111073. [Online]. Available: https://www.mdpi.com/2076-3417/12/21/11073 (visited on 01/03/2023).

[2] D. M. Wäresch, "Entwicklung eines Verfahrens zur dreiphasigen Zustandsschätzung in vermaschten Niederspannungsnetzen," de, p. 235,

[3] T. Jin and X. Shen, "A Mixed WLS Power System State Estimation Method Integrating a Wide-Area Measurement System and SCADA Technology," en, *Energies*, vol. 11, no. 2, p. 408, Feb. 2018, ISSN: 1996-1073. DOI: 10.3390/en11020408. [Online]. Available: https://www.mdpi.com/1996-1073/11/2/408 (visited on 01/04/2023).

[4] T. Matijašević, T. Antić, and T. Capuder, "A systematic review of machine learning applications in the operation of smart distribution systems," en, *Energy Reports*, vol. 8, pp. 12 379–12 407, Nov. 2022, ISSN: 2352-4847. DOI: 10.1016/j.egyr.2022.09.068. [Online]. Available: https://www.sciencedirect.com/science/article/pii/S2352484722017929 (visited on 03/13/2023).

[5] R. Brandalik, "Ein Beitrag zur Zustandsschätzung in Niederspannungsnetzen mit niedrigredundanter Messwertaufnahme," de, p. 223,

[6] Minyong Choi, Jinwoo Choi, Jonghoon Park, and Wan Kyun Chung, "State estimation with delayed measurements considering uncertainty of time delay," en, in *2009 IEEE International Conference on Robotics and Automation*, Kobe: IEEE, May 2009, pp. 3987–3992, ISBN: 978-1-4244-2788-8. DOI: 10.1109/ROBOT.2009.5152887. [Online]. Available: http://ieeexplore.ieee.org/document/5152887/ (visited on 03/09/2023).

[7] M. J. Tsatsomeros, "Principal pivot transforms: Properties and applications," en, *Linear Algebra and its Applications*, vol. 307, no. 1-3, pp. 151–165, Mar. 2000, ISSN: 00243795. DOI: 10.1016/S0024-3795(99)00281-5. [Online]. Available: https://linkinghub.elsevier.com/retrieve/pii/S0024379599002815 (visited on 10/09/2022).

[8] M. Rajesh Kannan and R. Bapat, "Generalized principal pivot transform," en, *Linear Algebra and its Applications*, vol. 454, pp. 49–56, Aug. 2014, ISSN: 00243795. DOI: 10.1016/j.laa.2014.04.015. [Online]. Available: https://linkinghub.elsevier.com/retrieve/pii/S0024379514002298 (visited on 10/19/2022).

[9] K. Kamaraj, P. S. Johnson, and S. M. Naik, "Generalized principal pivot transform and its inheritance properties," en, *The Journal of Analysis*, vol. 30, no. 3, pp. 1241–1256, Sep. 2022, ISSN: 2367-2501. DOI: 10.1007/s41478-022-00399-w. [Online]. Available: https://doi.org/10.1007/s41478-022-00399-w (visited on 11/02/2022).

[10] N. Amor, G. Rasool, and N. C. Bouaynaya, *Constrained State Estimation – A Review*, en, arXiv:1807.03463 [eess], Mar. 2022. [Online]. Available: http://arxiv.org/abs/1807.03463 (visited on 01/15/2023).

[11] S. Polster and H. Renner, "Berechnung elektrischer Energienetze," de, [Online]. Available: https://pure.tugraz.at/ws/portalfiles/portal/21042996/Berechnung_elektrischer_Energienetze_WS18_19.pdf (visited on 03/10/2023).